

Development of Full D-Band Corrugated Horn Antenna for ECRH System

Masatsugu SAKAGUCHI, Hiroshi IDEI¹⁾, Tetsuji SAITO and Takashi SHIGEMATSU

Furukawa C & B Co., Ltd., Yamato, Kanagawa 242-0018, Japan

¹⁾*Research Institute for Applied Mechanics (RIAM), Kyushu University, Kasuga, Fukuoka 816-8580, Japan*

(Received 16 May 2012 / Accepted 20 September 2013)

The corrugated horn antenna is widely used for the evaluation of transmission lines in electron cyclotron resonant heating systems, but little is known about the intensity and phase of its radiation profile over a wide frequency range. This paper is concerned with the development of a full D-band (110 - 170 GHz) corrugated horn antenna. The antenna was designed based on electromagnetic simulation codes for the finite element method and the method of moment. To verify these numerical simulations, a low-power test system was established, and its dynamic power range was defined for the precise measurement of antenna radiation. The fabricated antenna was measured and analyzed with basic Gaussian optics for a number of frequencies throughout the D-band. The measured radiation profiles are Gaussian-like and agree well with the numerical simulations. The radiated intensity pattern is slightly elliptical in the lower frequency range, as unwanted higher-order modes arose at the corrugated mode conversion section and generated the elliptical radiation pattern. The evolutions of the antenna radiation do not correspond with those expected by basic Gaussian optics.

© 2013 The Japan Society of Plasma Science and Nuclear Fusion Research

Keywords: corrugated horn antenna, finite element method, method of moment, basic Gaussian optics, radiation profile, mode conversion

DOI: 10.1585/pfr.8.1405163

1. Introduction

Nuclear fusion research is in the key process of constructing the flagship tokamak reactor, ITER, in Cadarache, France. ITER's aim is to show nuclear fusion can be used to generate electrical power, and to gain experimental data to design and operate the first electricity producing fusion power plant. The international fusion development program was widened to include a satellite tokamak within the Broader Approach (BA). JT-60SA (Naka, Japan) is a part of BA activities [1].

Electron Cyclotron Resonance Heating (ECRH) is an attractive method for plasma production, auxiliary heating, and current drive in a burning fusion-plasma experiments. The frequency of ECRH can be determined at either the fundamental or harmonics of the electron cyclotron frequency, $f_{ce} = neB/2\pi m_e \approx n \cdot 28$ [GHz/T] · [BT], where e and m_e are the electron charge and mass, B is the confinement magnetic field and $n = 1, 2, 3 \dots$ is the harmonic number. Accompanied by the magnetic field of the reactors, the ECRH frequency of ITER and JT-60SA is 170 GHz [2,3] and 110/137 GHz [4,5], respectively. Other than ITER and JT-60SA, many devices employ the ECRH system and have individual gyrotron frequency tied to long term R&D. Additionally, a dual frequency gyrotron have been studied for a future advanced ECRH system [6,7]. On the other hand, the frequency range is limited due to the gyrotron market for industries. The main frequency ranges

are 110 GHz band and 140 GHz band, 170 GHz band [8]. Multi frequency gyrotron will give a large flexibility to the ECRH system.

The present authors propose the use of a quasi-optical high-purity HE₁₁ mode exciter to experimentally evaluate the ECRH transmission line [9]. The HE₁₁ mode exciter is composed of a corrugated horn antenna and quasi-optical phase-matched mirrors. The corrugated horn antenna is widely used as a prime focus feed for high-efficiency reflector antennas in radio astronomy and radar, and it is also employed as a direct radiator in ECE radiometer applications. Although the corrugated horn antenna was a primary component of the HE₁₁ mode exciter, little is known about a number of its properties. One of these characteristics is the antenna's precise propagation profile, including both amplitude and phase. This profile is necessary to design the quasi-optical phase matched mirrors. The second property is the breadth of the antenna's bandwidth. A broadband standard antenna helps to evaluate the multifrequency ECRH devices throughout the full D-band range. The frequency range of commercial antennas separates several types of D-band range depending on the input circular waveguide radius.

In this paper, the development of a full D-band corrugated horn antenna is reported, focusing on the precise evaluation of its radiation properties and bandwidth. The contents of this paper are as follows: Section 2 reviews the general considerations of the corrugated horn antenna and

author's e-mail: sakaguchi.masatsugu@ho.furukawa-fcb.co.jp

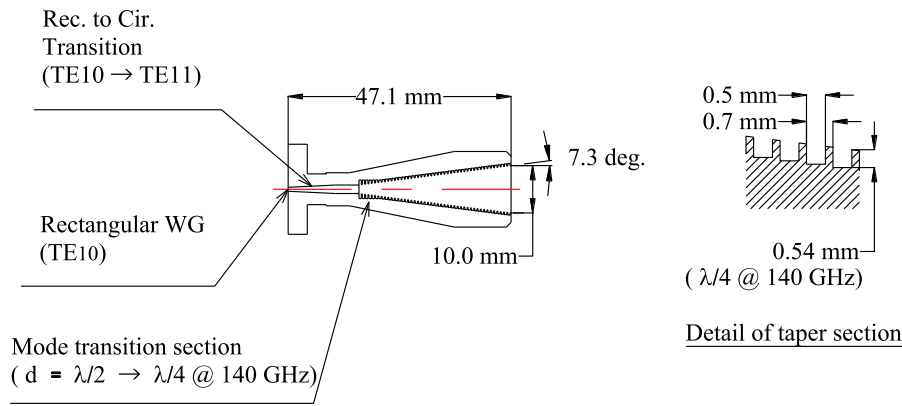


Fig. 1 Geometry and dimensions of the designed corrugated horn antenna.

describes the conceptual design of the antenna dimension; Section 3 describes the electromagnetic numerical simulations and their results; Section 4 describes the low-power test system for the measurement of antenna propagation; Section 5 describes the measurement results and the Gaussian optics analysis; and Sec. 6 is the summary.

2. General Considerations and Conceptual Design

Unwanted higher-order modes (HOMs) are easily excited in a normal smooth-wall horn antenna due to the edge diffraction related to the dominant mode. The excitation of HOMs can be eliminated by the addition of corrugating walls. Corrugated horns can provide reduced edge diffraction, improved pattern symmetry and reduced cross-polarization levels. When corrugations of width w and depth d are considered under conditions of $ka \gg 1$, the surface reactance at the open end is given approximately by the following equation [10]:

$$Z = \frac{w}{d} \tan(kd) \quad (1)$$

where $k(= 2\pi/\lambda)$ is the wave number and a is the radius of the antenna aperture. When the corrugation depth $d = \lambda/4$, Z becomes infinite, while when $d = \lambda/2$, Z becomes zero. The hybrid HE_{11} mode can be reached from the TM_{11} mode by increasing Z inductively from zero ($d = 0$ to $\lambda/4$) or from the TE_{11} mode by decreasing Z capacitively from zero ($d = \lambda/2$ to $\lambda/4$). Besides the above, a number of additional parameters determine the characteristics of the radiated modes, including the size of the smooth wall circular waveguide diameter, the length of the transition section and the aperture inner diameter. In particular, the shape of the corrugated wall section contributes to the broad bandwidth of the mode.

The operating principle of a corrugated horn antenna can be explained by considering the corrugated waveguide. The designed center frequency was 140 GHz, but the antenna was designed to work in the broadband frequency

range of the full D-band (110 - 170 GHz). After much deliberation, the geometry and dimensions were determined, as shown in Fig. 1. The input TE_{10} mode of the WR-6 fundamental rectangular waveguide was changed into the TE_{11} mode of the smooth-wall circular waveguide in the mode transition section. This section was individually designed using numerical simulations to eliminate the potential propagation of HOMs (TM_{01} and TE_{21} mode). The converted TE_{11} mode led into another mode transition section with corrugations. The corrugated walls linearly flared for simplicity and consisted of a mode launching section and a taper section. The mode launching section changed from an initial depth of $\lambda/2$ to a final depth of $\lambda/4$ at 140 GHz, and the taper section had a constant depth of $\lambda/4$. The aperture inner diameter contributed to the radiated beam size and was arbitrarily selected as 10.0 mm. The length of the corrugated walls, including those of the mode launching section, was determined automatically according to the selected taper angle and the aperture diameter. A longer and smoothly flared mode launching section is desired for a broader bandwidth. The spread angle of the walls was set at 7.3 degrees due to manufacturing limitations.

The propagation properties can be approximated with Gaussian optics in association with the mode conversion efficiency of the free-space Gaussian beam and the HE_{11} mode. The beam waist radius w_0 and waist location z are approximated below [11]:

$$w_0 = \frac{0.6435a}{1 + \left[\frac{\pi(0.6435a)^2}{\lambda R_h} \right]^2} \quad (2)$$

$$z = \frac{R_h}{1 + \left[\frac{\lambda R_h}{\pi(0.6435a)^2} \right]^2} \quad (3)$$

where R_h is the horn slant length and a is the aperture radius.

3. Numerical Simulations

3.1 Comparison between numerical simulation codes

To verify the conceptual design, we employed two types of electromagnetic numerical simulation codes and observed the differences between them. The first was the HFSS (ver. 13.0) code for the finite element method (FEM), and the other was the Wipl-d (ver. 9.0) code [12] for the method of moment (MoM). The FEM uses a precise volume mesh and is common in antenna analysis, particularly in examining near-field resonance conditions. However, the FEM requires substantial CPU time to solve due to its volume mesh, including the propagating free space area. MoM requires relatively little CPU time because of its surface meshing, and it is mainly used in the analysis of large-scale free-space propagation.

Following these conceptual designs, the geometry of the antenna could be modeled and analyzed at frequencies of 110 GHz, 140 GHz and 170 GHz. The MoM simulation model and the fabricated antenna resulting from the numerical simulation are shown in Fig. 2. The parts of the antenna were divided into the smooth-wall waveguide sec-

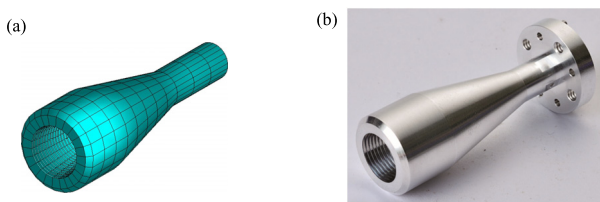


Fig. 2 (a) Simulation model in MoM and (b) fabricated antenna. The fabricated antenna was manufactured by the direct machining of aluminum.

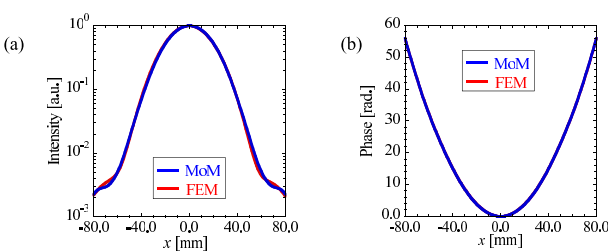


Fig. 3 (a) Intensity and (b) phase profiles of the corrugated horn antenna as simulated by MoM and FEM along the x -direction ($z = 150$ mm, 140 GHz).

tion and the corrugation section and were manufactured using a computerized numerical control machining center.

Using the FEM and MoM simulations, the propagation characteristics of the antenna were calculated at various propagation positions. In these results, the z -axis is the propagation direction, and the origin of the z coordinate was the position of the antenna aperture; however, this was an artificial position. The direction of y was designated by the copolarization following the direction of the rectangular waveguide. In Fig. 3 (a), the intensity profiles of both simulations were nearly identical within the dynamic range of 20 dB. The phase profiles of both codes were also similar, as shown in Fig. 3 (b). The propagation profiles were consistent between the codes at every frequency, but there was a major difference in calculation time, as shown in Table 1. A vast amount of CPU time was spent to calculate the field radiating from the antenna in the FEM simulation due to the expansion of the tiny mesh according to the shorter wavelength, particularly at the highest frequency (170 GHz). The MoM code was employed for the development of the antenna primarily for its CPU time advantage.

3.2 Simulation results

By using the MoM simulation with the designed antenna dimensions, the propagated waves could be analyzed for a variety of frequencies. The amplitude profiles of the E_x and E_y components along the x - and y -direction are shown in Fig. 4. The cross-polarization discrimination was extremely good, and the E_x component of cross polarization was negligible.

The intensities of the electric fields at a variety of frequencies and a distance of $z = 50$ mm propagated from the antenna aperture are shown in Fig. 5. The oblateness of the radiation patterns in Fig. 5 is shown in Table 2. Oblateness was determined in the range of $1.0w$ to $1.3w$. As seen in Fig. 5 and Table 2, the patterns were symmetrical around the propagation axis. The pattern was slightly elliptical on the outside of the beam radius w at the lowest frequency. For this reason, two mode transition sections were numerically investigated, because the HOMs of these sections might have an effect on the elliptical beam pattern. One of mode transition sections converted the rectangular TE_{10} to the circular TE_{11} mode, and the other was the corrugated mode transition section in which the corrugation depth changed linearly from $\lambda/2$ to $\lambda/4$ at 140 GHz. First, the content of the TE_{11} mode at the first mode transition section was analyzed using the FEM code, as shown

Table 1 CPU time in the designed antenna simulations.

	110 GHz	140 GHz	170 GHz
FEM	512 s	1790 s	5825 s
MoM	113 s	158 s	223 s

OS: Windows 7 Pro 64 bit
 CPU: Intel Core i7 3.2GHz
 RAM: 24GB
 GPU accelerator ×3, supported in MoM

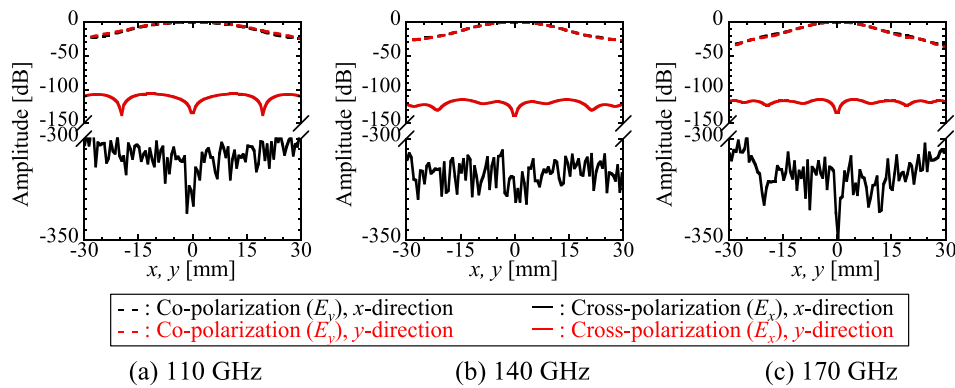


Fig. 4 MoM-simulated copolarization (E_y component) and cross polarization (E_x component) amplitude patterns at $z = 50$ mm in the H plane (along the x -direction) and E plane (along the y -direction).

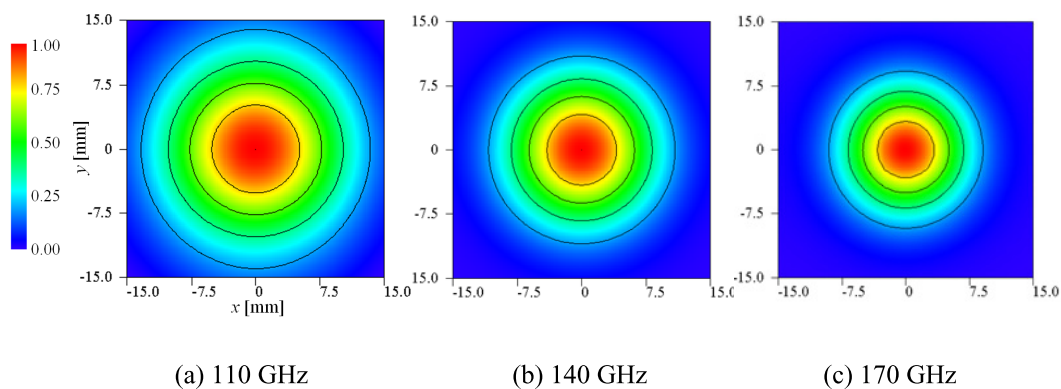


Fig. 5 Intensity field pattern calculated by MoM simulation at $z = 50$ mm in a range of a 30 mm square focusing on the beam center at frequencies of (a) 110 GHz, (b) 140 GHz and (c) 170 GHz.

Table 2 Oblateness of radiation pattern measured at $z = 50$ mm.

Range	110 GHz	140 GHz	170 GHz
1.0w	0.04	0.02	0.01
1.3w	0.11	0.02	0.03

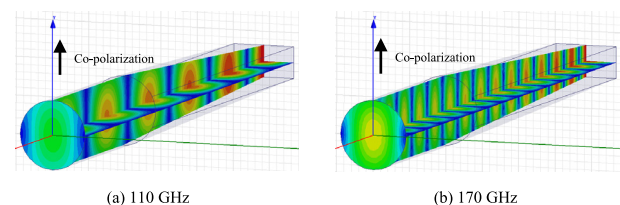


Fig. 6 Cross-sectional E/H plane surface amplitude distribution in the rectangular-circular mode transitional section at (a) 110 GHz and (b) 170 GHz.

in Fig. 6. The content of each mode can be calculated by eigenmode expansion in HFSS. The highest content of the TE_{11} mode was 99.2% (at 110 GHz). At the other frequencies, the mode contents were 97.8% (at 140 GHz) and 97.6% (at 170 GHz). These results indicate that the rectangular to circular transition contributed relatively little to the HOMs of the corrugated horn antenna. Next, the propagation of the corrugated part, which included the second mode transitional section, was analyzed using MoM, as shown in Fig. 7. At 110 GHz, the amplitude level by the inner wall was higher towards the horn aperture on the yz plane (E plane) compared with the xy plane (H plane). This result suggests that the diffraction was caused by the

edges of the corrugations and that the standing wave arose from the combination of reflection and interference at the corrugated mode transitional section on the yz plane (E plane). The amplitude distributions were similar between the E and H planes, exhibiting no diffraction at 170 GHz.

The elliptic radiation patterns at the lower frequencies were due to the nonoptimized corrugated mode transitional section. The nonoptimized mode transition caused the standing waves and diffraction. The functional form of the corrugated mode transitional section should be considered in the future work, but a linear shape was employed

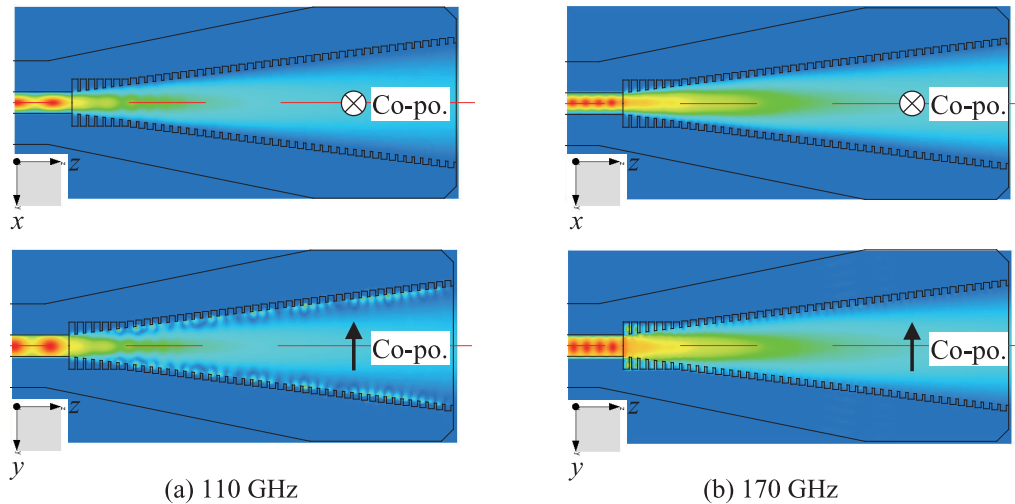


Fig. 7 Cross-sectional E/H plane surface amplitude distribution in the corrugated section at (a) 110 GHz and (b) 170 GHz.

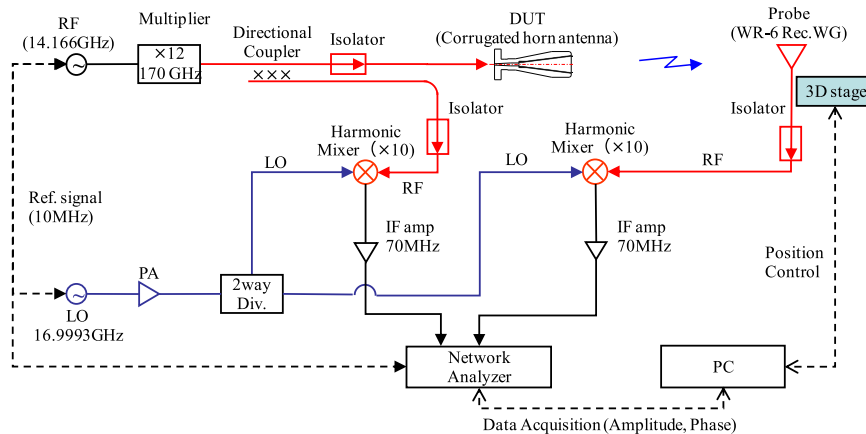


Fig. 8 Schematic diagram of the low-power measuring system.

in the present study.

4. Experimental Setup

4.1 Experimental geometry

The low-power measuring system for the propagating waves was prepared in collaboration with Kyushu University, as shown in Fig. 8 and Fig. 9. The test system was composed of millimeter wave components and a receiver (WR-6 rectangular waveguide), which was controlled by a three-dimensional stage to scan the measuring point. The accuracy of positioning the receiver stage was on the order of 1/100 of the wavelength of the frequency range. Figure 8 shows a schematic diagram of the system at 170 GHz. Two synthesizers were prepared to obtain a stable, high-resolution measuring frequency. The first was a radio frequency (RF) source used as a multiplier to generate the millimeter wave, and the second was a local (LO) oscillator used for its harmonic mixers. The LO signals were equally divided and led to the reference port and receiver

port. Because the conversion loss in the harmonic mixers was not low (typically 35 dB), additional intermediate frequency (IF) amplifiers were prepared. The IF signals were connected to the vector network analyzer (Agilent Technologies 8753ES) and detected at 70 MHz. The properties of the propagated wave were measured by comparing the reference signal with the received spatial scanned signal.

4.2 Test of the low-power measuring system

To verify the low-power measuring system, the phase evolution of the propagated wave was measured. The system required an accurate alignment setting between the propagating z direction and the system longitudinal direction. HOMs can be excited due to the misalignment of the propagating axis in the waveguide coupling between the corrugated waveguides. A misalignment of 1 degree has been shown to generate unwanted mode contents of 0.03 [13].

The receiver was shifted along the z direction away

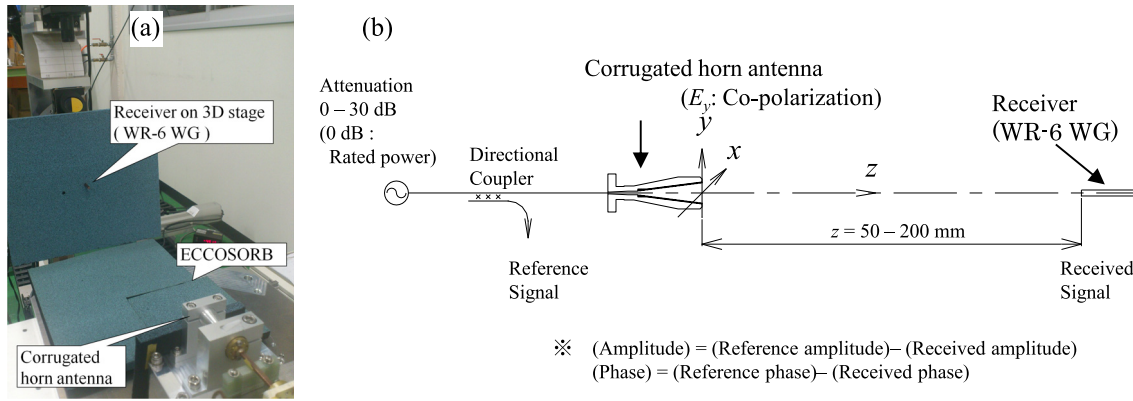


Fig. 9 (a) Experimental setup (corrugated horn and the receiver fixed on the 3D stage) and (b) experimental diagram.

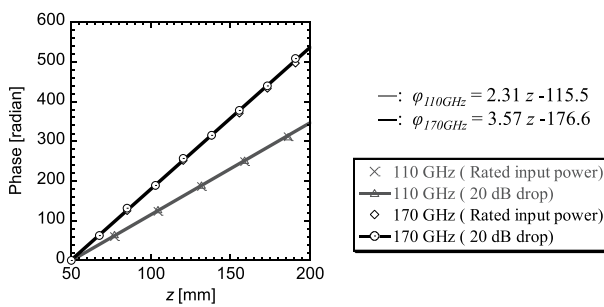


Fig. 10 Measured phase evolution along the z -direction in the system test.

from the antenna aperture in increments of approximately 10λ , as shown in Fig. 9. The measured frequencies were 110 GHz and 170 GHz, and the input RF power level was intentionally decreased by 20 dB to 40 dB from the rated input power level. Figure 10 shows the measured phase evolutions at each level and the linearization lines for the input power drop of 20 dB. The measured plots were nearly identical at every power range and well approximated to the linearization lines. The phase evolution was expressed with the kz term. The gradient of the linearization lines agreed well with the theoretical wave numbers k ($k = 2.305$ at 110 GHz and $k = 3.563$ at 170 GHz), even as the input power dropped by 20 dB. Additionally, the dynamic range was checked by attenuating the input signal when the receiver position was fixed at $z = 200$ mm. The measured amplitude level is shown in Fig. 11, and the received level at $z = 50$ mm was characterized as the reference signal level. As the power was reduced in 5 dB increments, the receiving level also fell linearly and was under the noise level when the attenuation level was 30 dB. These results indicated that the test system was correctly aligned and possessed a dynamic range at a power of approximately 25 dB.

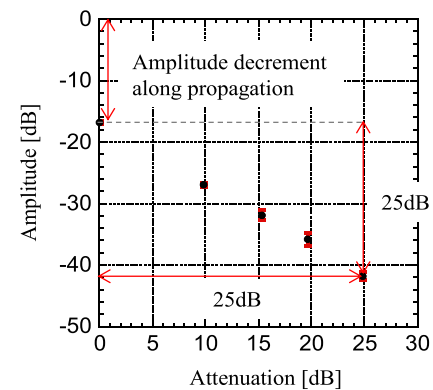


Fig. 11 Measured amplitude level when the input signal was attenuated at $z = 200$ mm.

5. Experimental Results and Discussion

5.1 Gaussian-like beam

The intensity and phase distributions radiating from the horn antenna were measured at $z = 50$ to 200 mm in increments of 50 mm at 110 GHz and 170 GHz. It should be noted that the phase offset from the finite receiving angle was not taken into consideration by the receiver's (WR-6 rectangular waveguide) radiation properties. The phase differences around beam center were minor: 0.024 radian in the E plane and 0.055 radian in the H plane. Figure 12 shows the contour plots of the measured intensity and phase patterns at a propagating length of $z = 50$ mm and a frequency of 170 GHz. Both phase profiles were symmetric, without an offset toward the beam center. The antenna propagation axis was well aligned to the axis of the system longitudinal direction. The intensity profile was symmetric at 170 GHz but was elliptical, as predicted by the MoM simulation, at 110 GHz.

The validity of the numerical simulations was checked using experimental data from the low-power measuring system. Figure 13 shows the measured intensity and phase

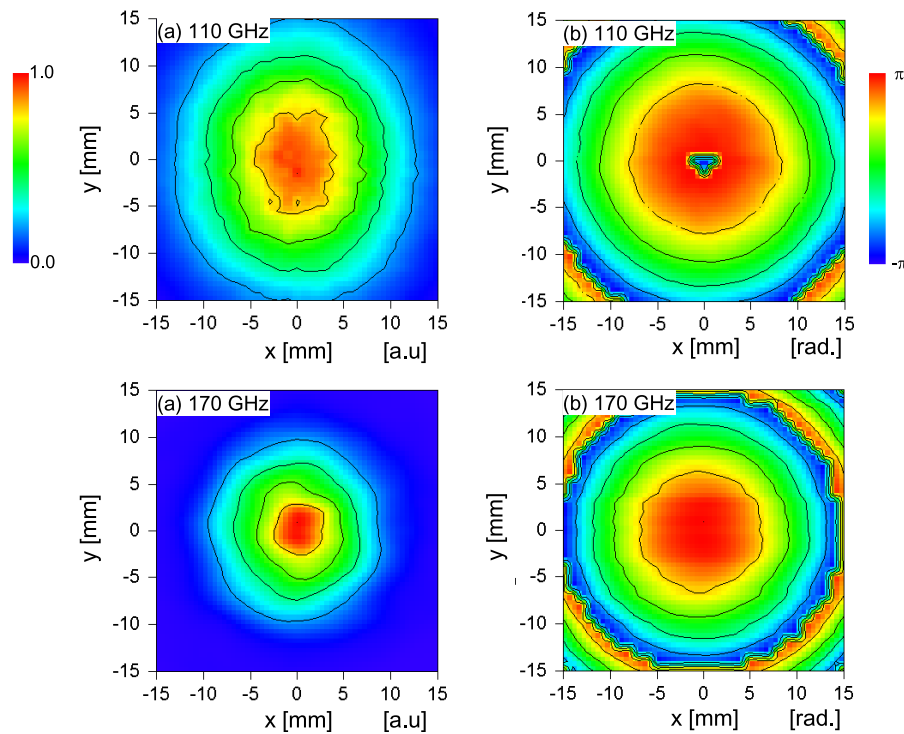


Fig. 12 Measured (a) intensity and (b) phase patterns of the horn antenna ($z = 50$ mm, 110 and 170 GHz).

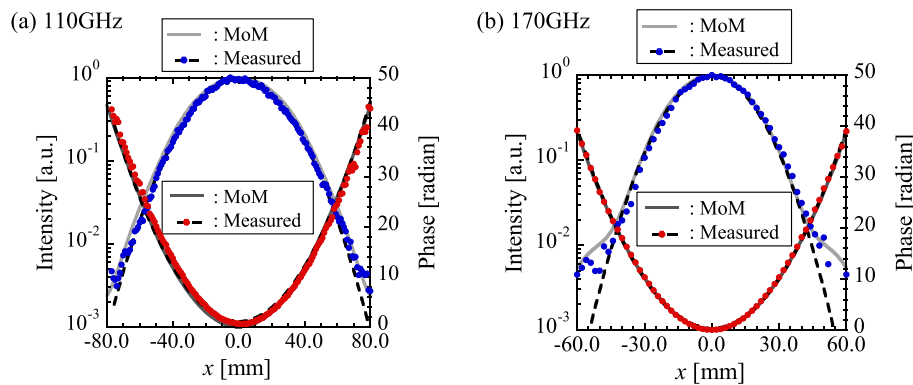


Fig. 13 Measured intensity and phase profiles with the fitted curves along the x -direction at $z = 150$ mm at frequencies of (a) 110 GHz and (b) 170 GHz. The MoM simulation results for the same conditions are also indicated.

distribution at $z = 150$ mm, with the fitted curve calculated using Gaussian optics and the MoM-simulated distribution also marked. The measured intensity profile was Gaussian-like at the dynamic range of 20 dB in both frequencies. This agreement was sufficient because an intensity drop of 20 dB or a beam radius of $1.52 w$ includes 99% of the radiated power. The measured and simulated profiles exhibited a strong agreement. The MoM simulation showed good agreement with the measurements, proving itself to be a useful tool for designing millimeter wave components in free-space propagation.

5.2 Basic Gaussian optics analysis

To determine the beam evolution, all profiles were fitted and analyzed in terms of basic Gaussian optics. Figure 14 shows the evolution of the beam radius in the x and y axes along the propagating z direction. The Gaussian beam parameters (w_0, z_0) were deduced from Fig. 14 and are noted in Table 3. The evolutions of the phase curvature R are shown in Fig. 15, along with the fitted and analyzed curves. The analyzed curves were calculated from the parameters shown in Table 3. In addition, the Gaussian beam parameters (w_0, z) of the antenna were deduced from Eq. (2) and (3): (w_0, z) = (2.94 mm, 3.31 mm) at 110 GHz and (w_0, z) = (2.63 mm, 3.31 mm) at 170 GHz.

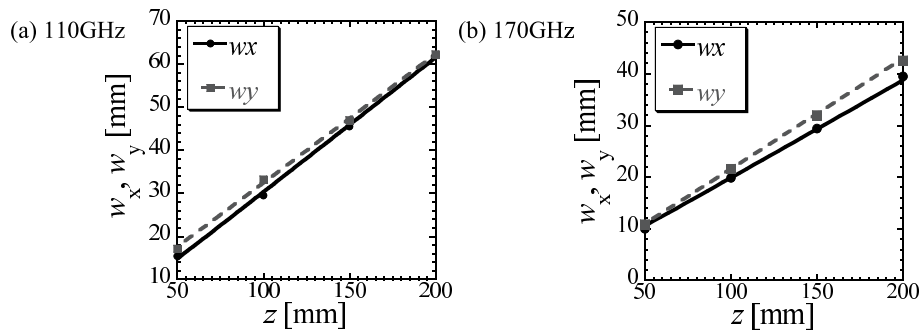


Fig. 14 Measured beam radius evolutions along the propagating z -axis at frequencies of (a) 110 GHz and (b) 170 GHz.

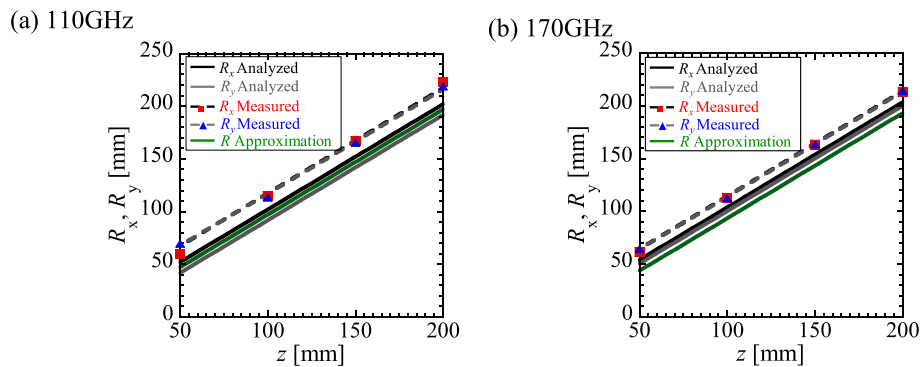


Fig. 15 Measured and analyzed phase curvature evolutions along the propagating z -axis at frequencies of (a) 110 GHz and (b) 170 GHz. The analyzed curves were calculated from the parameters shown in Table 3.

Table 3 The beam waist radius and the positions analyzed from measured beam radius evolutions.

	w_{0x} [mm]	w_{0y} [mm]	z_{0x} [mm]	z_{0y} [mm]
110 GHz	3.06	2.14	-1.62	8.52
170 GHz	2.84	2.64	-15.3	-0.94

These parameters reflected the phase curvature evolutions in Fig. 15. The Gaussian beam parameters differ between the measured amplitude and the phase evolution in Fig. 15. The approximate evolution also differed from the measured evolutions. These results indicate that basic Gaussian optics cannot express the beam propagation of the horn antenna. Amplitude control techniques such as phase-matched mirrors are necessary to excite a pure Gaussian beam.

6. Summary

The broadband corrugated horn antenna was developed for various uses in nuclear fusion research. The propagation profiles of such antennas should be evaluated for both amplitude and phase. The antenna used in the present study was evaluated using numerical simulations and ex-

perimental measurements. First, the antenna was designed and fabricated using the method of moment and the finite element method. The bandwidth was broad, but the radiation patterns were slightly elliptical in the lower frequencies of the D-band (110 - 170 GHz). The cause of this ellipticity was likely the unwanted higher-order modes arising at the mode conversion section. Next, a low-power measuring system was constructed and tested to validate the numerical simulations. The measured intensity and phase distributions at 110 GHz and 170 GHz were in good agreement with the simulation results. The radiation properties were Gaussian-like and applicable for broadband use, but these evolutions did not correspond with basic Gaussian optics. The results indicate that precise radiation profiles are manageable using numerical simulations and low-power measurement, and such management will assist the design of phase-matched mirrors.

Acknowledgments

This work was realized in the collaboration between Furukawa C & B Co., Ltd. and Kyushu University.

[1] M. Kikuchi *et al.*, 21st IAEA Fusion Energy Conference, 1-9 (2006).
 [2] F. Gandini *et al.*, Fusion Sci. Technol. **59**, 709 (2010).
 [3] T. Omori *et al.*, Fusion Eng. Des. **86**, 951 (2011).

- [4] S. Moriyama *et al.*, Nucl. Fusion **49**, 8 (2009).
- [5] A. Isayama *et al.*, Plasma Fusion Res. **7**, 2405029 (2011).
- [6] D. Wagner *et al.*, IEEE Trans. Plasma Sci. **36**, 2, 324 (2008).
- [7] K. Sakamoto *et al.*, International Conference on Infrared, Millimeter, and Terahertz Waves, 1 (2011).
- [8] V. Erckmann *et al.*, AIP Conf. Proc. **1406**, 165 (2011).
- [9] H. Idei *et al.*, Proceedings of US/Japan/EU RF Heating Technology Workshop, 1 (2011).
- [10] J.D. Kraus, *Antennas 2nd ed.* (McGraw-Hill Companies, New York, 1988) p.657.
- [11] P. Goldsmith, *Quasioptical Systems: Gaussian Beam Quasioptical Propagation and Applications* (IEEE Press, New York, 1998) p.170.
- [12] B.M. Kolundžija *et al.*, *WIPL-D Microwave: Circuit and 3D EM Simulation for RF & Microwave Applications* (Artech House, London, 2005) p.2.
- [13] H. Idei *et al.*, IEEE Trans. Microw. Theory Tech. **54**, 11 (2006).